# Nanostructure of Fluorocarbon Films Deposited on Polystyrene from Hyperthermal $C_3F_5^+$ Ions

**F. Ahu Akin,[†,‡] Inkook Jang,[§] Mark L. Schlossman,*[,†,||] Susan B. Sinnott,[§] Gerry Zajac,[⊥] Erick R. Fuoco,[†] Muthu B. J. Wijesundara,[†,○] Ming Li,[||,#] Aleksey Tikhonov,[||,▽] Sai Venkatesh Pingali,[||] Amanda T. Wroble,[†] and Luke Hanley*[,†]**

*Departments of Chemistry and Physics, University of Illinois at Chicago, Chicago, Illinois 60607-7061, Department Materials Science & Engineering, University of Florida, Gainesville, Florida 32611-6400, and BP Chemicals Research Center, 150 W. Warrenville Road., Naperville, Illinois 60566*

*Received: July 21, 2003; In Final Form: March 1, 2004*

Fluorocarbon films were grown on polystyrene in vacuum from 25- to 100-eV mass-selected $C_3F_5^+$ ion beams. The films were analyzed by X-ray photoelectron spectroscopy, atomic force microscopy, and X-ray reflectivity after exposure to the atmosphere for 4−8 weeks. The X-ray reflectivity indicates films that range from ∼30 to 60-Å thick. The thinner films form at lower ion energies, where the ion penetration depth and efficiency of film formation are lowest. X-ray reflectivity estimates air−fluorocarbon film roughness values of ∼6 Å for 25- and 50-eV films but ∼20 Å for the 100-eV films. The fluorocarbon−polystyrene-buried interface displays similar roughness and trends with ion energy. The AFM roughness trends are similar, but the absolute AFM roughnesses are only $\sim^1/_4$ of the X-ray reflectivity values. This discrepancy is attributed to tip effects and the method of determining roughness by AFM. The AFM images and power spectral densities of the 100-eV films displayed quasi-periodic cones spaced 300−700 Å apart. Such features are either absent or of much lower amplitude in the 25- and 50-eV films. Classical molecular dynamics simulations of $C_3F_5^+$ deposition on polystyrene at energies of 50 and 100 eV/ion reveal that etching at the higher energy is largely responsible for the dissimilar film structures obtained experimentally. These results demonstrate that deposition of the fluorocarbon polyatomic ion $C_3F_5^+$ allows control of film nanostructure at the surface and buried interface.

## I. Introduction

Controlling and determining the nanostructure of disordered organic thin films is critical to a variety of applications. However, the absence of crystallinity limits the use of diffraction-based methods for the structural determination of disordered organic films. Their susceptibility to radiation damage limits the use of electron microscopy. Their film thickness and buried interface structure are not readily observed by scanning probe microscopy. However, a combination of techniques can circumvent these limitations to obtain a detailed picture of the organic film's surface topology, thickness, buried interface structure, and electron density. This paper combines X-ray reflectivity[1−4] and atomic force microscopy (AFM) to determine the nanostructure of fluorocarbon films on polystyrene substrates. The fluorocarbon films studied here are produced by the deposition of mass-selected 25−100-eV $C_3F_5^+$ polyatomic ions. This paper also applies molecular dynamics simulations to explain how the deposition of these polyatomic fluorocarbon ions controls the nanostructure of these films.

Several groups have shown that specific chemical functionality can be imparted to a surface by depositing polyatomic ions with controlled kinetic energy and fluence.[5−7] Our previous work prepared 25−100-eV $C_3F_5^+$ ion-deposited fluorocarbon films and analyzed them both before and after air exposure.[8−10] We found that hyperthermal $C_3F_5^+$ ions formed a distribution of different fluorocarbon moieties on polystyrene in amounts that were dependent upon the incident ion energy and fluence. We deposited 25-eV $C_3F_5^+$ ions mostly intact on the surface to form fluorocarbon films with some degree of cross linking. The fragmentation and fluorination efficiency of the $C_3F_5^+$ ions increased with projectile ion energies of 50 and 100 eV. Exposure to air for 4−8 weeks led to the appearance of an oxygen content of several percent because of the oxidation of the radical sites formed during ion bombardment. Air exposure was necessitated by the period required for the serial preparation of multiple films and their subsequent transport to the synchrotron light source for analysis.

Polyatomic ion deposition is also attractive because it can be readily modeled by computer simulations. Molecular dynamics and Monte Carlo simulations of ion−surface interactions are straightforward because the ion masses, their kinetic energy, and their fluence are all well defined.[5,11] Molecular dynamics simulations of hyperthermal $C_3H_5$[8,12] and $C_3F_5$[13] modifications of polystyrene provided mechanistic information on the aforementioned experimental results for the fluorocarbon film growth. The surface nanostructuring will be discussed in terms of the new simulation results presented here.

* Corresponding authors. (L.H.) E-mail: lhanley@uic.edu. (M.L.S.) E-mail: schloss@uic.edu.
[†] Department of Chemistry, University of Illinois at Chicago.
[‡] Current address: Department of Chemistry, University of Nevada Reno, Reno, Nevada 89557.
[§] University of Florida.
[||] Department of Physics, University of Illinois at Chicago.
[⊥] BP Chemicals Research Center.
[○] Current Address: Department of Chemical Engineering, University of California, Berkeley, California 94720.
[#] Current address: Institute of Physics, Chinese Academy of Sciences, Beijing 100080, P. R. China.
[▽] Current address: University of Chicago, Center for Advanced Radiation Sources, and NSLS Beamline X19C, Brookhaven National Laboratory, Upton, New York 11973.

10.1021/jp036129n CCC: $27.50 
Published on Web 06/12/2004

Previous studies have shown that ion fluence can control the coverage of fluorocarbon films deposited on polystyrene and poly(methyl methacrylate).[8,14] The behavior of the C(1s) and F(1s) core-level peak intensities in XPS also indicated that the ion energy controlled the morphology, but the nature of this morphological change was not determined.[8] X-ray reflectivity, XPS, and AFM are combined here to demonstrate how ion kinetic energy determines the fluorocarbon film thickness and nanostructure, both at the surface and the buried interface. Portions of the X-ray reflectivity, AFM, and XPS data presented here have been published previously.[10,15] However, this paper provides a more complete structural analysis of the films by comparing the X-ray reflectivity data with the power spectral densities of the AFM data.[16] Furthermore, the molecular dynamics simulations provide a mechanistic explanation of the dependence of nanostructuring on the ion energy that is observed by X-ray reflectivity and AFM.

## II. Experimental Details

**A. Film Preparation and Ion Beam Conditions.** Film preparation and ion beam conditions have been previously described and will only be summarized here.[8,10] Approximately 270-Å-thick polystyrene films were spin coated onto Si(100) wafers from a 0.3% polystyrene (molecular weight: 4600 Da, Aldrich) solution in $CH_2Cl_2$ for 1 min at 6000 rpm. Survey and valence band X-ray photoelectron spectra confirmed the cleanliness of the surface and the uniformity of the polystyrene film. Different samples were used for the various analyses (see below), and two to four samples were analyzed by each method. Error bars on the data represent either the standard deviation for the analysis of different data sets (X-ray photoelectron spectroscopy) or the uncertainty in analyzing single data sets (X-ray reflectivity), whichever is greater.

The apparatus used for mass-selected ion−surface modification and surface analysis consists of a differentially pumped low-energy ion source, a preparation chamber, and an analysis chamber. $C_3F_5^+$ ions were formed from $C_3F_6$ vapor by 80-eV electron impact ionization, accelerated, mass selected by a Wien filter, decelerated to 25−100-eV kinetic energy, refocused, and transmitted at normal incidence to the polystyrene sample mounted in the preparation chamber. A low-energy electron flood gun was used to minimize surface charging during ion exposure, and the preparation chamber pressure was $\sim 8 \times 10^{-8}$ Torr during film preparation. Typical ion currents were 15−20 nA, and ion fluences were equivalent to $1.0 \times 10^{16}$ F atoms/cm$^2$. The samples were then removed from the UHV chamber and aged by storage in a desiccator for 4−8 weeks prior to analysis.

**B. X-ray Photoelectron Spectroscopy (XPS).** Details of the XPS experiments and data analysis have been disclosed previously and are only summarized here.[8] XPS was performed with a high-resolution monochromatic Al K$\alpha$ X-ray source (15 keV, 25-mA emission current, model VSW MX10 with a 700-mm Rowland circle monochromator, VSW Ltd., Macclesfield, Cheshire, U.K.) and a 150-mm concentric hemispherical analyzer (model class 150, VSW Ltd.) with a multichannel detector operated in constant energy analyzer mode. The photoelectron takeoff angle was normal to the surface, and the pass energy was 22 eV, which gives 0.75-eV energy resolution for the Ag ($3d_{5/2}$) peak on a sputter-cleaned Ag foil. The C(1s) (aliphatic/aromatic) core-level peak of native polystyrene was assigned to 285.0 eV and used as a charge reference for all of the other photoemission peaks.

**C. X-ray Reflectivity.** X-ray reflectivity was conducted at beamline X19C at the National Synchrotron Light Source (Brookhaven National Laboratory) with measurement techniques described in detail elsewhere.[3,4] The kinematics of reflectivity is illustrated in Figure 1.

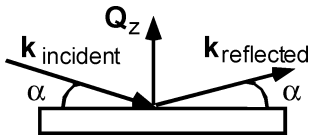


**Figure 1.** Kinematics of X-ray reflectivity. $Q_z = (4\pi/\lambda)\sin(\alpha)$ is the wave-vector transfer normal to the surface.

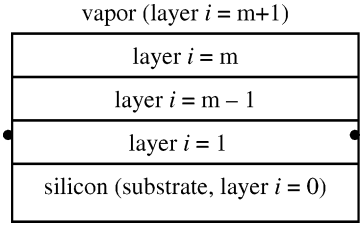


**Figure 2.** Nomenclature for layers used in modeling X-ray reflectivity data.

For specular reflection, the wave-vector transfer, $\mathbf{Q} = \mathbf{k}_{\text{reflected}} - \mathbf{k}_{\text{incident}}$, is only in the $z$ direction, normal to the surface; $Q_x = Q_y = 0$, where $x$ and $y$ are in the plane of the surface, and $Q_z = (4\pi/\lambda)\sin(\alpha)$ with the X-ray wavelength $\lambda = 1.540 \pm 0.0008$ Å. Therefore, specular reflection probes the structure normal to the surface. Specifically, specular reflectivity probes the electron density normal to the surface and averaged over the region of the X-ray footprint on the sample. The reflectivity data consist of measurements of the X-ray intensity reflected from the sample normalized to the incident intensity measured just before the X-rays strike the surface. These data are further modified by subtracting a background measured slightly off the specular condition by averaging intensity values at wave-vector transfer $\mathbf{Q} = (0, \Delta Q_y, Q_z)$ and $\mathbf{Q} = (0, -\Delta Q_y, Q_z)$.[4] An incident slit (a gap varying from 5 to 20 $\mu$m with the angle of incidence) determines the beam size on the sample, and a slit (gap = 2 mm) before the detector sets the resolution of the measurement.

The samples were placed in a vapor-controlled aluminum chamber with Kapton X-ray windows. The chamber was flushed with clean helium gas and a low flow of helium across the sample was maintained during the X-ray measurements. The X-ray measurements could be reproduced by immediately measuring a second set of data after the first set, indicating that radiation damage did not influence our measurements. However, it is interesting that if the samples were removed from the He cell, not exposed to X-rays for a period of 24 h and then replaced in the cell, a significant change in the data was recorded when the sample was remeasured. This degradation of the polystyrene films upon removal from the He cell likely occurred via reaction with atmospheric oxygen from the radicals formed by X-ray damage.

The samples are modeled as a series of layers on top of the silicon substrate, with nomenclature defined in Figure 2. Each layer has an interface width that describes the smooth crossover of the electron density of the layer to that of its neighboring layers. For example, the thin polystyrene film of the untreated sample is modeled as a single layer with a different interface width at its vapor interface and at the interface with the silicon surface. Adsorbed fluorocarbon, due to the treatment of the film with energetic $C_3F_5^+$ ions, is modeled by an additional layer of different electron density on top of the polystyrene layer. For data at large enough $Q_z$ it may be necessary to include a thin layer of silicon oxide between the silicon and the polystyrene.

A general formula for the electron density gradient of a sample with $m$ layers is[2]

$$\left\langle \frac{d\rho}{dz} \right\rangle = \sum_{0}^{m} (\rho_i - \rho_{i+1}) \frac{1}{(2\pi\sigma_{i+1}^2)^{1/2}} e^{-(z - D_i)^2/2\sigma_{i+1}^2} \qquad (1)$$

where $\rho_o$ is the electron density of the silicon substrate, $\rho_{m+1}$ is the density in the vapor, and $D_i = \sum_{j=1}^{i} L_j$ is the distance from the surface of the silicon substrate to the surface between the $i$th and $(i+1)$ layers, where $L_i$ is the thickness of the $i$th layer and $\sigma_{i+1}$ is the interfacial width between the $i$th and $(i + 1)$ layers.

Given the electron densities of each layer and the subphase as well as the widths for each interface, the specular reflectivity is calculated using the Parratt formalism.[17] The comparison of the calculated reflectivity to the data and adjustment of the fit parameters allows the data to be fit using a standard-fitting algorithm. In the Parratt formalism, the exact reflection and transmission coefficients for each interface are used to calculate the specular reflectivity. We employed a modified version of that formalism in which an error function is used to model a smooth crossover from the electron density of one layer to its neighboring layer (as indicated by the Gaussian describing the density gradient as in eq 1). As described below, the fit parameters correspond to qualitative features of the data.

**D. AFM.** The surface morphology of the fluorocarbon films was measured with an atomic force microscope (model Nanoscope IIIA, Digital Instruments, Santa Barbara, CA) equipped with tapping mode and phase contrast for highest spatial resolution. Tapping mode was used to avoid sample damage. Four $1 \times 1$-$\mu m^2$ areas were scanned for each ion and energy. The rms roughness was calculated for each spot using the instrumental software, and the average was taken for each sample. Tapping mode AFM images from the 50- and 100-eV samples and rms roughness values have been previously published.[10] Two-dimensional power spectral densities (PSD) of each image were also taken using the Nanoscope SPM software (v. 5.12, Veeco Metrology Group). Height images were auto-plane fit (second order, *xy*) and then flattened (second order). Four PSDs were averaged together to create representative PSD plots for the surfaces at each ion energy.

## III. Computational Details

The classical molecular dynamics (MD) simulations undertaken here numerically integrate Newton's equations of motion with a third-order Nordsieck predictor corrector[18] using a time step of 0.2 fs. Short-range interatomic forces are calculated using a new carbon−hydrogen−fluorine potential based on the second-generation reactive empirical bond-order potential[19] described in detail elsewhere.[20] Long-range van der Waals interactions are included in the form of a Lennard−Jones potential that is active only at distances greater than the covalent bond lengths.[18] These potentials are empirical and classical, which means that electronic effects such as electronic excitations or charging of the atoms are not included. Thus, ions with positive charges are treated as reactive radicals rather than true ions with an actual charge. Although the presence of a positive charge will undoubtedly influence the chemical reactions that occur during deposition, it is also true that most if not all incident ions are rapidly neutralized as they approach the surface, making this a reasonable approach.

The polymer surface used in the simulations is syndiotactic crystalline polystyrene that has a total thickness of 50 Å. The three bottom layers of the surface and atoms within 5−10 Å from the four sides of the slab have Langevin frictional forces[18] applied to maintain the surface temperature at 300 K. This allows the polystyrene slab to imitate the heat dissipation that occurs in the much larger experimental surfaces. The rest of the atoms in the system have no constraints and are designated as active. Periodic boundary conditions are also applied within the plane of the surface to mimic an infinite surface and effectively double the number of thermostat atoms at the edges of the surface.

The simulations consider the continuous deposition of a beam of 105 $C_3F_5^+$ ($CF_2-C^+F-CF_2$) ions at 100 and 50 eV/ion of kinetic energy. Each ion in the beam is deposited at a randomly chosen location within the active region of the surface at random orientations relative to the surface. The incident angle is normal to the surface, and the total fluence in each case is $0.8 \times 10^{16}$ F atom/cm$^2$. After the deposition processes are complete, the systems are fully equilibrated for 20 ps.

**TABLE 1: Elemental Percentages of Native Polystyrene and 25−100-eV $C_3F_5^+$ Ion-Deposited Fluorocarbon Films on Polystyrene Surfaces[10]**

| element | pure polystyrene | 25 eV | 50 eV | 100 eV |
|---|---|---|---|---|
| carbon | 100 | 79 ± 4 | 50 ± 4 | 56 ± 2 |
| fluorine | | 19 ± 3 | 46 ± 2 | 38 ± 1 |
| oxygen | | 3 ± 1 | 4 ± 1 | 6 ± 2 |

**TABLE 2: C(1s) Component Percentages of 25−100-eV $C_3F_5^+$ Ion-Modified Polystyrene[a]**

| binding energy (eV) | component(s) | pure polystyrene | 25 eV | 50 eV | 100 eV |
|---|---|---|---|---|---|
| 285.0 | $CH_n$ | 95 | 87 ± 2 | 32 ± 2 | 40 ± 2 |
| 286.2 | $\underline{C}CF_n$, C−O | | 9 ± 2 | 35 ± 2 | 38 ± 3 |
| 288.7 | $\underline{C}FCF_n$, C═O, O−C═O | | | 20 ± 0 | 14 ± 1 |
| 291.1 | $CF_2$ | 5($\pi - \pi^*$) [b] | 4 ± 0.1 | 12 ± 1 | 7 ± 0.1 |
| 293.3 | $CF_3$ | | | 1 ± 0.3 | 1 ± 0.1 |

[a] Possible components are displayed for each binding energy[10] [b] Native polystyrene displays a $\pi-\pi^*$ transition occurring near 291 eV, where no fluorocarbons are observed for the native sample. The $\pi-\pi^*$ transition occurs near and is obscured by $CF_2$ and/or $CF_3$ groups in the fluorocarbon films.

## IV. Experimental Results

**A. Elemental and Chemical Content of Fluorocarbon Films.** The elemental and chemical contents of the ion-deposited fluorocarbon films have been presented previously[10] and are summarized in Tables 1 and 2. The fluorocarbon films display 20−50% fluorine and 3−6% oxygen, with the remainder being carbon. (Hydrogen is not detected by XPS.) The oxygen resulted from aging in air for 4−8 weeks. Fluorine and oxygen content increase with ion energy because of the enhanced fragmentation of both the $C_3F_5^+$ ion and the polystyrene, as well as increased reaction with atmospheric oxygen and water. Additional information on the ion-modified film chemistry was obtained by peak fitting the C(1s) spectra, shown in Table 2. The 25-, 50-, and 100-eV samples display different amounts of various fluorocarbon and oxygenated components, including $CH_n$, $\underline{C}CF_n$, C−O, $\underline{C}FCF_n$, C═O, O−C═O, $CF_2$, and $CF_3$ (underlined C detected). The peak assignments and widths used to fit the C(1s) spectra were $CH_n$ (aliphatic/aromatic) at 285.0 eV (0.95-eV fwhm); $\underline{C}CF_n$ and C−O at 286.2 eV (1.9 eV); $\underline{C}FCF_n$, C═O, and O−C═O at 288.7 eV (1.8 eV); $CF_2$ at 291.1 eV (1.4 eV); and $CF_3$ at 293.3 eV (1.4 eV). The changes

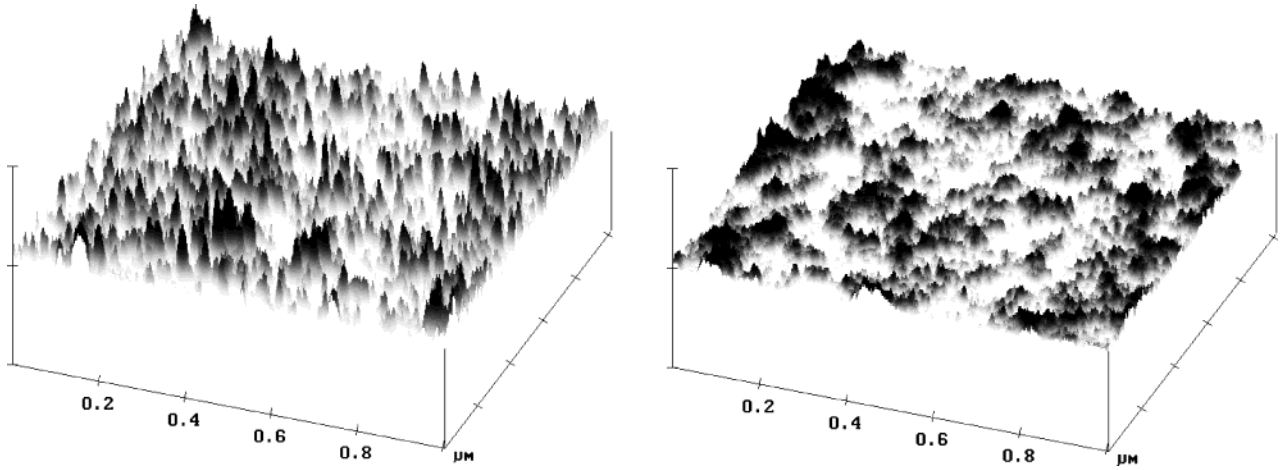


**Figure 3.** Tapping mode AFM images from a 1 $\mu$m × 1 $\mu$m area of 100-eV $C_3F_5^+$ (left) and 25-eV $C_3F_5^+$ (right) ion-deposited films on polystyrene substrates. *Y*-axis increments are 3 nm. Images are artificially shadowed to emphasize 3D structure.

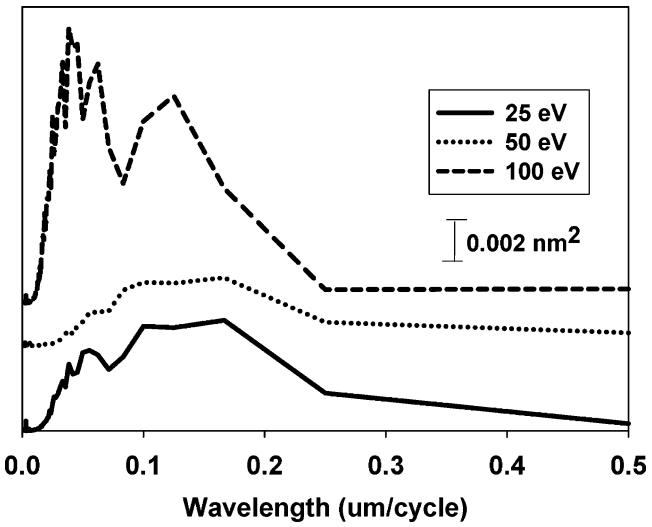


**Figure 4.** Averaged power spectral densities (PSDs) of AFM images of fluorocarbon films deposited at 25, 50, and 100 eV.

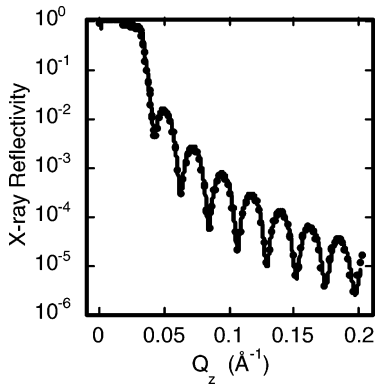


**Figure 5.** X-ray reflectivity data (points) and fit (solid line) as a function of wave-vector transfer normal to the silicon surface for a pure polystyrene layer spin coated onto a silicon wafer.

reported for the C(1s) components in Table 2 result mostly from variations in the pure fluorocarbon component percentages and, to a lesser extent, changes in the degree of oxidation.[8,10] For example, the 25-eV samples display lower fractions of $\underline{C}CF_n$ and $CF_2$ as well as no $\underline{C}FCF_n$ fraction, when compared with the 50- and 100-eV samples. The chemical differences in the fluorocarbon films are expected from their electron densities. (See below.)

**B. AFM.** Figure 3 displays tapping mode AFM images for 100- and 25-eV samples (left and right, respectively). Differently shaped features with sizes in the hundreds of angstrom range are observed for all ion-modified surfaces, with quasi-periodic conical structures that appear prominently in the 100-eV samples. The AFM images of the 50-eV samples (not shown)[10] were similar to the those of 25-eV samples. The rms roughness of the 100-eV samples was much higher than that of the other samples, at 7.4 ± 0.6 Å. By contrast, the rms roughness values of the 25- and 50-eV samples were 2.4 ± 0.2 and 1.8 ± 0.2 Å, respectively. By contrast, the roughness of the unmodified polystyrene surface was 1.0 ± 0.2 Å, and its AFM images were featureless.

The PSDs of the AFM images are shown in Figure 4. All PSDs displayed features at 0.1−0. 3 $\mu$m/cycle, although these features were the most intense for the 100-eV surfaces. The 100-eV surfaces additionally displayed relatively strong features at 0.03−0.07 $\mu$m/cycle. These features are likely due to the quasi-periodic conical structures observed in the AFM spectra of the 100-eV samples (Figure 3, left). The overall higher intensities of all PSD features for the 100-eV samples versus those of the lower-energy samples are consistent with their greater roughnesses. The use of PSDs for quantifying AFM images has been previously defended in cases such as this, where the image features can be constructed from a summation of sine wave functions.[16]

**C. X-ray Reflectivity.** *Pure Polystyrene.* X-ray reflectivity for a pure polystyrene layer spin coated onto a silicon wafer is shown in Figure 5. The oscillations are due to coherent interference between X-rays reflected from the polystyrene−vapor interface and the silicon−polystyrene interface. This pure polystyrene layer is fit using a single-layer model, yielding a layer thickness of 275 Å with a normalized electron density of $\rho_{PS}/\rho_{Si} = 0.455$, where the electron density of the silicon is $\rho_{Si} = 0.696$ e$^-$/Å$^3$. The value for $\rho_{PS}$ is comparable to that deduced from the literature value for the mass density of 1.0 g/cm$^3$, which corresponds to $\rho_{\text{literature polystyrene}}/\rho_{Si} = 0.46$.[1] The vapor interface roughness or width is 5.5 Å, and the polystyrene−silicon interface roughness is 2.7 Å. The latter value was taken from other measurements (to be discussed) at a higher $Q_z$ because the measurement in Figure 5 is not very sensitive to that width. The critical $Q$ for total reflection that was used to fit all of the data sets is 0.0318 Å$^{-1}$, in agreement with the calculated value. The small step below the critical angle indicates that these measurements also probed the critical angle for total reflection from the polystyrene. To fit below the critical angle of silicon

**TABLE 3: Parameters for Fits of X-ray Reflectivity Data[a]**

| | | pure PS | 25 eV | 50 eV | 100 eV |
|---|---|---|---|---|---|
| | | Layer Thickness $L_j$ (Å) | | | |
| $SiO_2$ | $L_1$ | | | | $10 \pm 1$ |
| polystyrene (PS) | $L_2$ | $275.2 \pm 0.5$ | $272 \pm 2$ | $272 \pm 4$ | $258 \pm 3$ |
| fluorocarbon | $L_3$ | | $33 \pm 3$ | $25 \pm 3$ | $60 \pm 5$ |
| | | Electron Density $\rho_j/\rho_{Si}$ | | | |
| $SiO_2$ | $\rho_1/\rho_{Si}$ | | | | 0.96[b] |
| PS | $\rho_2/\rho_{Si}$ | $0.455 \pm 0.015$ | 0.45[b] | $0.45 \pm 0.02$ | $0.47 \pm 0.1$ |
| fluorocarbon (FC) | $\rho_3/\rho_{Si}$ | | $0.515 \pm 0.025$ | $0.54 \pm 0.02$ | $0.68 \pm 0.05$ |
| | | Interfacial Width (Roughness) $\sigma_{ij}$ **(Å)** | | | |
| $Si/SiO_2$ or Si/PS | $\sigma_{01}$ | 2.7[b] | $3.4 \pm 0.3$ | $2.7 \pm 0.1$ | 1[b] |
| $SiO_2$/PS | $\sigma_{12}$ | | | | $2.55 \pm 0.15$ |
| PS/FC or PS/vapor | $\sigma_{23}$ | $5.5 \pm 0.5$ | $3 \pm 3$ | $5 \pm 2$ | $18 +6/-3$ |
| FC/vapor | $\sigma_{34}$ | | $6.8 \pm 0.5$ | $6.3 \pm 0.5$ | $22.5 \pm 2$ |

[a] Samples are polystyrene spin coated on silicon, then bombarded with $C_3F_5^+$ ions at energies of 25, 50, and 100 eV. Electron densities, $\rho$, are normalized by $\rho_{Si}$, where $\rho_{Si} = 0.696$ e$^-$/Å$^3$. Other parameters used in the fit include the critical $Q$ for total reflection from silicon, $Q_C = 0.0318$ Å$^{-1}$, and x-ray absorption lengths of 0.104 cm for the polystyrene and 0.0066 cm for the silicon. Blank values indicate layers not used for those samples. (The layer numbering must be adjusted accordingly.) [b] Parameters kept fixed during fitting.

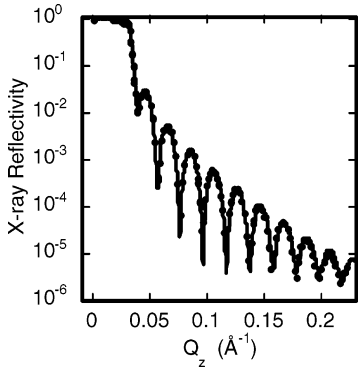


**Figure 6.** X-ray reflectivity data (points) and fit (line) as a function of wave-vector transfer normal to the silicon surface for a spin-coated polystyrene layer on silicon exposed to 25-eV $C_3F_5^+$ ions.

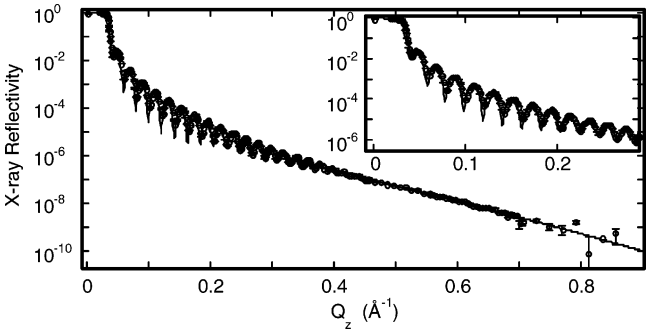


**Figure 7.** X-ray reflectivity data (points) and fit (line) as a function of wave-vector transfer normal to the silicon surface for a spin-coated polystyrene layer on silicon exposed to 50-eV $C_3F_5^+$ ions. The inset is a detail of the low $Q_z$ region.

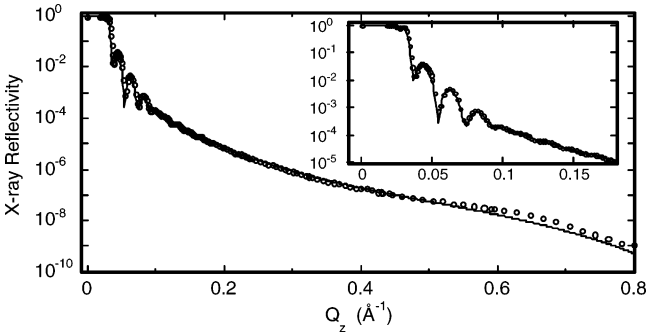


**Figure 8.** X-ray reflectivity data (points) and fit (line) as a function of wave-vector transfer normal to the silicon surface for a spin-coated polystyrene layer on silicon exposed to 100-eV $C_3F_5^+$ ions. Error bars are smaller than the open circles. The inset is a detail of the low $Q_z$ region.

requires the use of an absorption length of 0.104 cm for the polystyrene and 0.0066 cm for the silicon, both values taken from standard X-ray tables. The fit parameters are summarized in Table 3.

*25-eV Sample.* The data and fit for the X-ray reflectivity of a 25-eV sample are shown in Figure 6,[15] and the fit parameters are listed in Table 3. These data cannot be adequately fit by a one-layer model of polystyrene. If so fit, then the amplitude of the oscillations shows a systematic deviation that indicates the presence of another layer. The fit for the 25-eV sample is a two-layer model. The polystyrene layer is similar to the layer on the pure polystyrene sample, indicating that it is probably unaltered by exposure to the $C_3F_5^+$ ions. On top of the polystyrene layer is a 33-Å-thick layer of higher electron density than polystyrene. We attribute this to the slightly oxidized fluorocarbon, whose electron density, $\rho_F = 0.515\ \rho_{Si}$, is much less than the value measured for close-packed, unoxidized fluoroalkanes ($0.9\ \rho_{Si}$)[21]

*50-eV Sample.* Figure 7 illustrates the X-ray reflectivity for a 50-eV sample. The fit parameters are listed in Table 3. The polystyrene thickness is the same as that of the pure polystyrene and the 25-eV samples, indicating that fluorocarbon exposure probably does not alter the underlying polystyrene. The fluorocarbon layer is similar in thickness but with slightly larger electron density than that of the 25-eV sample. The vapor interface has a roughness of 6 Å, also similar to the 25-eV sample.

*100-eV Sample.* Figure 8 illustrates the X-ray reflectivity for a 100-eV sample. The fit parameters are listed in Table 3. The falloff in reflectivity at higher $Q_z$ indicates the presence of a thin silicon oxide layer on the substrate. The fluorocarbon layer is much thicker and of higher electron density than those of the 25- and 50-eV samples. The vapor interface is much rougher, consistent with the AFM observations. Also, the interface between the fluorocarbon layer and the polystyrene is much rougher. The presence of these rougher interfaces is indicated qualitatively by the loss of oscillations in the reflectivity at the relatively low $Q_z \approx 0.1$ Å$^{-1}$. Finally, the polystyrene layer thickness is 258 Å, ~10 Å thinner than in the other three cases.

*Real-Space Profiles.* The electron density normal to the silicon surface is illustrated in Figure 9 for the four samples just discussed. It is clearly seen that the 25- and 50-eV samples are very similar, whereas the 100-eV treatment results in a greater deposition of fluorocarbon.

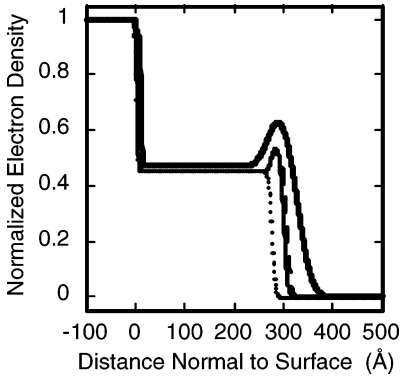


**Figure 9.** Electron density (normalized to the value for bulk silicon, $\rho_{Si} = 0.696\ e^{-}/Å^3$) as a function of the distance normal to the silicon substrate (negative values are into the silicon substrate). The dotted line is the untreated polystyrene sample (bottom trace), the dashed line is the 25-eV sample (middle trace), the thin solid line is the 50-eV sample (middle trace), and the thick solid line is the 100-eV sample (top trace).

## V. Computation Results

The MD simulations reveal important differences in the deposition process as the energy of the incident ion beam is changed from 50 to 100 eV/ion. Figure 10 shows part of the polystyrene surfaces from simulations after the $C_3F_5^+$ ion beam deposition at 100 and 50 eV. Many fluorocarbon ions and dissociated ion fragments are embedded in the polystyrene with or without covalent bonding to the polystyrene carbon atoms. The ordered polymer structures are randomized and swelled by ion bombardment. Because of the higher ion velocity, ion deposition with 100 eV of kinetic energy induces more disordering of the polystyrene than ion deposition at 50 eV. In addition, significantly more etching of the polystyrene surface occurs at 100 eV/ion. Surface etching yields are 1.10 C atoms/ion and 1.30 H atoms/ion at 100 eV and 0.28 C atom/ion and 0.28 H atom/ion at 50 eV. Although ion bombardment at 100 eV induces more surface damage, the total F uptake and deposition yield are higher at 100 eV than at 50 eV. For instance, F uptakes are $4.61 \times 10^{15}$ F atoms/cm$^2$ and $2.72 \times 10^{15}$ atoms/cm$^2$ for deposition at 100 and 50 eV, respectively. Deposition yields of the F atom are 57.7 and 34.1% for deposition at 100 and 50 eV, respectively. More incident ions are simply scattered away from the polystyrene surface during deposition at 50 eV/ion.

Figure 11 shows almost the whole polystyrene surface and depth profiles of F densities after the ion deposition process is complete. The cause of the apparent negative depth is the swelling of the polystyrene surfaces (zero depth is the initial level of the pristine surfaces). The F atoms spread more widely and deeply at the 100-eV deposition. The average penetration depths are 19.2 Å for C and 18.6 Å for F atoms after deposition at 100 eV/ion and 17.3 and 17.2 Å for C and F, respectively, in the case of deposition at 50 eV/ion. The highest density of F occurs at a depth of 15−20 Å for both 100- and 50-eV/ion deposition processes.

Tables 4 and 5 show the surface density of the indicated species formed from the incident $C_3F_5^+$ ions that remain at the polystyrene surfaces after deposition at 100 and 50 eV, respectively. A more diverse sampling of ion fragments is formed at 100 eV, and more of these fragments form covalent bonds to the polystyrene than is the case for deposition at 50 eV. This is highlighted by the fact that at 100 eV very few intact $C_3F_5$ groups survive deposition; however, they are the most abundant species formed at 50 eV. Despite this increased dissociation of the incident ions at 100 eV, a significant number of large species that consist of more than three carbon atoms are observed at this energy. These large species are important precursors of fluorocarbon polymer films.

In addition, a large number of fluorine atoms covalently bonded to the carbon atoms of polystyrene chains are found in

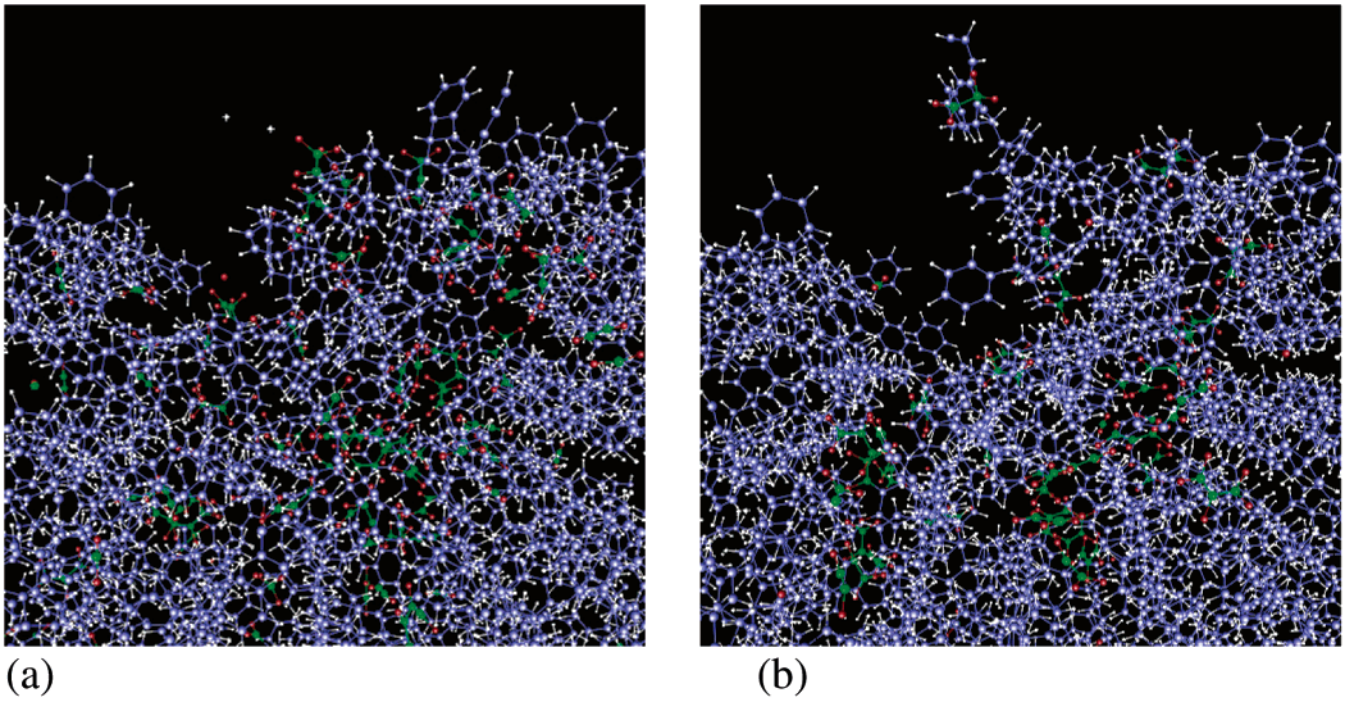


**Figure 10.** Structure models of part of the polystyrene surfaces (red spheres are F atoms, green spheres are C atoms from the ions, blue spheres are C atoms from the polystyrene, and white spheres are H atoms). Snapshot of the polystyrene surface after deposition at (a) 100 eV/ion and (b) 50 eV/ion.

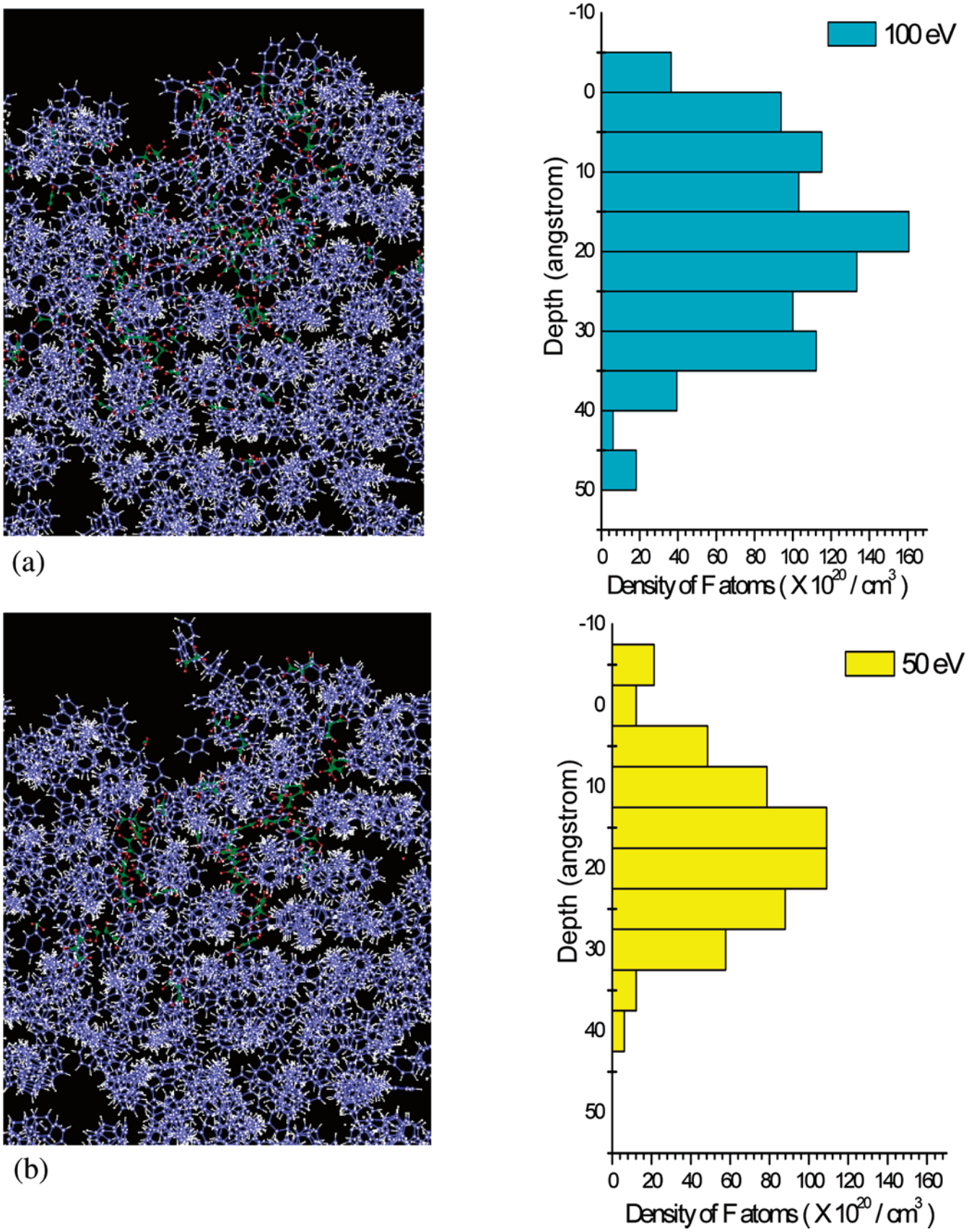


**Figure 11.** Structure models of polystyrene surfaces. Snapshot of the polystyrene surface after deposition at (a) 100 eV/ion and (b) 50 eV/ion. Depth profiles of F density in the polystyrene surface are shown to the right of each snapshot. The vertical scales of the depth profile graphs are matched to the snapshots. The negative depth corresponds to swelling of the polystyrene surfaces, as discussed in the text. Zero depth is the initial surface level of the pristine surfaces.

100-eV deposition, and most of these F atoms replace hydrogen atoms in the polystyrene chains. However, only a few fluorine atoms are observed in 50-eV deposition. Therefore, the $C_3F_5^+$ beam deposition at 100 eV is more efficient for the fluorination

**TABLE 4: Surface Density of Indicated Species that Remain Bonded to Carbon Atoms In, or Are Embedded within, the Polystyrene Surfaces after $C_3F_5^+$ Deposition at 100 eV/ion[a]**

| | density ($\times 10^{13}$ cm$^{-2}$) | |
|---|---|---|
| | covalently bonded | embedded |
| $C_3F_5$ | 0 | 6.1 |
| $C_3F_n$ (except $C_3F_5$) | 1.5 | 6.1 |
| $C_2F_2$ | 0 | 28.9 |
| $C_2F_n$ (except $C_3F_5$) | 12.2 | 18.2 |
| $CF_2$ | 21.8 | 19.8 |
| $CF_n$ | 7.6 | 13.7 |
| $C_nF_m$ ($n > 3$, $m > 5$) | 9.1 | 1.5 |
| F | 56.2 | 12.2 |

[a] Embedded means the species are embedded in, but not bonded to the surface on the time scales of the simulations.

**TABLE 5: Surface Density of Indicated Species that Remain Bonded to Carbon Atoms In, or Are Embedded within, the Polystyrene Surfaces after $C_3F_5^+$ Deposition at 50 eV /Ion**

| | density ($\times 10^{13}$ cm$^{-2}$) | |
|---|---|---|
| | covalently bonded | embedded |
| $C_3F_5$ | 1.5 | 28.9 |
| $C_3F_n$ (except $C_3F_5$) | 0 | 3.0 |
| $C_2F_n$ | 4.6 | 9.1 |
| $CF_2$ | 4.6 | 10.6 |
| CF | 3.0 | 1.5 |
| $C_nF_m$ ($n > 3$, $m > 5$) | 1.5 | 1.5 |
| F | 1.5 | 12.2 |

of the polystyrene substrate than that of the 50 eV. However, surface damage is more severe in 100-eV deposition.

## VI. Discussion

**A. Summary of Results.** The combined results of X-ray reflectivity and AFM data draw a detailed picture of the nanostructure of these fluorocarbon films. The X-ray reflectivity indicates a film thickness ranging from ~30 to 60 Å, with thinner films forming at lower ion energies.[8] X-ray reflectivity estimates an air−fluorocarbon film roughness of ~6 Å for 25- and 50-eV films but ~20 Å for the 100-eV films. The fluorocarbon−polystyrene buried interfaces display similar trends in roughness with ion energy. The AFM roughness trends are similar, but the absolute AFM roughnesses are only ~$^1/_4$ of the X-ray reflectivity values. The AFM images and PSDs of the 100-eV films displayed quasi-periodic cones spaced 300−700 Å apart (Figure 3, left). Such features are either absent or of much lower amplitude in the 25- and 50-eV films (Figure 3, right). The X-ray reflectivity results cannot confirm or dispute the quasi periodicity because they are not sensitive to in-plane homogeneities.

The MD simulations indicate the manner in which the chemical modification of polystyrene surfaces through $C_3F_5^+$ deposition is similar and different at 50 and 100 eV/ion. For instance, the penetration depth of ion fragments is similar at the two energies. However, deposition at 100 eV induces more disordering and ~4× higher etching of the polystyrene. Furthermore, F atoms and ion fragments are more readily formed at 100 eV. Finally, fluorocarbon−polystyrene covalent bonding, fluorocarbon deposition, and surface damage are all greater at 100 eV. By contrast, unreacted scattering of incident ions is greater at 50 eV.

**B. Mechanisms of Film Nanostructuring.** The computer simulations indicate that the competitive processes of etching and deposition are the primary mechanisms by which 100-eV $C_3F_5^+$ forms nanostructures on the polystyrene surface. The simulations indicate that etching is ~4× higher at 100 eV than at 50 eV. Furthermore, $C_3F_5^+$ is twice as likely to dissociate to reactive F atoms at 100 eV than at 50 eV. Other reactive fragments are also more easily formed from the parent ion at the higher energy. Surface damage, including polystyrene bond cleavage, is also higher at 100 eV. These fragments and F atoms are more effective at both etching and fluorinating polystyrene than intact $C_3F_5^+$ species. The latter leads to overall thicker fluorocarbon films at 100 eV. As the polystyrene is etched away and replaced with fluorocarbon, nanostructures are formed. X-ray reflectivity shows an ~10-Å reduction in the underlying polystyrene film thickness at 100 eV compared to that for 25- and 50-eV ion-modified (as well as native) films, which indicates large-scale etching of the polystyrene by the fluorocarbon ion deposition, although questions regarding the reproducibility of the initial polystyrene film thickness (~270 Å) prevent a more quantitative experimental determination of etching. Polystyrene bond cleavage and etching at 100 eV is further indicated by film oxidation and aging effects,[10] the known etching ability of small fluorocarbon fragments at elevated ion energies[22] and experimental evidence on related systems.[23]

The simulations at 50 eV indicate less etching, more intact $C_3F_5^+$ deposition, and more scattering off the surface. The reduced etching apparently leads to the formation of the smoother fluorocarbon films observed experimentally at 50 eV. The thinner fluorocarbon films observed experimentally at 50 eV are consistent with the lower-efficiency ion film formation observed in the 50-eV simulations. No simulations were performed at 25-eV incident ion energies, but the 50-eV trends of less ion fragmentation and less etching are expected[8] to lead to the same relatively smooth films observed experimentally at 25 eV. Ion and fragment penetration depths are less important than etching in nanostructuring because they are only a few percent higher for 100-eV ion impacts. Penetration depths are similar from 50 to 100 eV because most of the kinetic energy is dissipated by the first ion−surface collision.

The computer simulations are very useful in elucidating the role of fast processes such as etching, penetration, and bond formation/cleavage. However, these simulations do not account for several longer-term effects that might also contribute to nanostructuring. First, the oxidation of the fluorocarbon films, indicated by the few-percent oxygen, cannot be probed by the potential functions applied here. Nanostructuring might manifest itself at least partially through the oxidation of fragments to form volatile species. Furthermore, the segregation of the deposited films into fluorocarbon/hydrocarbon regions might also be occurring and might be enhanced at 100 eV by more polystyrene bond breakage. However, the much longer time scale of such a diffusional process is not accessible to these simulations.

**C. Discrepancies in X-ray Reflectivity and AFM Data.** The comparison of the two experimental probes of organic film morphology demonstrated both their relative strengths and their complementary nature. The X-ray reflectivity and AFM display similar trends but different absolute values of roughness. This discrepancy is attributed to tip effects in the AFM, which will tend to smooth over finer features and reduce the measured roughness. Also, questions have been raised regarding the accuracy of standard rms roughness values determined by AFM,[16] despite their widespread use. X-ray reflectivity was found to be the most accurate and provides an absolute measure of the film electron density, roughness, and thickness normal

to the surface. However, such high-resolution X-ray reflectivity measurements require access to a source of synchrotron radiation. AFM provided a more approximate but nevertheless useful estimate of surface morphology and film thickness using instrumentation that is widely available.

## VII. Conclusions

These results demonstrate that the deposition of the fluorocarbon polyatomic ion $C_3F_5^+$ allows for control of the film nanostructure at the surface and buried interface of thin polystyrene films. Ions (25- and 50-eV) form smoother, thinner films of lower electron density, and 100-eV ions form thicker, rougher films of higher electron density. The kinetic energy of mass-selected $C_3F_5^+$ ions control the film's morphology by mediating the competing processes of surface etching, film formation, ion fragmentation, ion penetration into and damage of the substrate, reactions between deposited ions and/or the substrate, sputtering, etching, and diffusion. In particular, the simulations indicate that nanostructuring arises by F atoms and $C_xF_y$ fragments that preferentially form at 100 eV and more effectively etch the surface than the intact $C_3F_5$ species that tend to survive surface impact at 50 eV. Differences in ion penetration depths, although slightly higher at 100 than at 50 eV, do not appear to explain the nanostructuring that is predominant only at the higher ion energy.

Polyatomic ion deposition is a highly flexible method for controlling both surface nanostructure and chemistry.[5] Other examples of control of the nanoscale film morphology by mass-selected polyatomic ion deposition have been previously discussed.[15,22] Mass-selected ion deposition experiments are directly comparable to MD simulations but are practical only for small-area film growth.[8,9,12,24,25] A non-mass-selected polyatomic ion deposition process has also been demonstrated to allow control of the film's morphology and rapidly produce nanostructured films over much larger areas.[15] Control of the film's nanostructure is also feasible using the related method of surface polymerization by ion-assisted deposition (SPIAD), which combines polyatomic ion deposition with the simulaneous evaporation of neutral organic species.[26]

**Acknowledgment.** This work is supported by the U.S. National Science Foundation through grant CHE-9986226 (L.H.), DMR-0092469 (M.L.S), and CHE-0200838 (S.B.S.). The X-ray reflectivity experiments were performed at the National Synchrotron Light Source on beamline X19C, Brookhaven National Laboratory, which is supported by the U.S. Department of Energy. Dr. William Lackowski of TAMU, Chemistry Department, Texas A&M University, is acknowledged for his assistance in power spectral processing of the AFM images.

## References and Notes

(1) Russell, T. P. *Mater. Sci. Rep.* **1990**, *5*, 171.
(2) Tidswell, I. M.; Ocko, B. M.; Pershan, P. S.; Wasserman, S. R.; Whitesides, G. M.; Axe, J. D. *Phys. Rev. B* **1990**, *41*, 1111.
(3) Schlossman, M. L.; Pershan, P. S. X-ray and Neutron Scattering from Liquid Surfaces. In *Light Scattering by Liquid Surfaces and Complementary Techniques*; Langevin, D., Ed.; Marcel Dekker: New York, 1992; p 365.
(4) Schlossman, M. L.; Synal, D.; Guan, Y.; Meron, M.; Shea-McCarthy, G.; Huang, Z.; Acero, A.; Williams, S. M.; Rice, S. A.; Viccaro, P. J. *Rev. Sci. Instrum.* **1997**, *68*, 4372.
(5) Hanley, L.; Sinnott, S. B. *Surf. Sci.* **2002**, *500*, 500.
(6) Wade, N.; Evans, C.; Jo, S.-C.; Cooks, R. G. *J. Mass Spectrom.* **2002**, *37*, 591.
(7) Evans, C.; Wade, N.; Pepi, F.; Strossman, G.; Schuerlein, T.; Cooks, R. G. *Anal. Chem.* **2002**, *74*, 317.
(8) Wijesundara, M. B. J.; Ji, Y.; Ni, B.; Sinnott, S. B.; Hanley, L. *J. Appl. Phys.* **2000**, *88*, 5004.
(9) Wijesundara, M. B. J.; Hanley, L.; Ni, B.; Sinnott, S. B. *Proc. Natl. Acad. Sci. U.S.A.* **2000**, *97*, 23.
(10) Wijesundara, M. B. J.; Zajac, G.; Fuoco, E.; Hanley, L. *J. Adhes. Sci. Technol.* **2001**, *15*, 599.
(11) Garrison, B. J.; Kodali, P. D. S.; Srivastava, D. *Chem. Rev.* **1996**, *96*, 6, 1327.
(12) Jang, I.; Phillips, R.; Sinnott, S. B. *J. Appl. Phys.* **2002**, *92*, 3363.
(13) Jang, I.; Sinnott, S. B. *Appl. Phys. Lett.*, in press.
(14) Wijesundara, M. B. J.; Fuoco, E.; Hanley, L. *Langmuir* **2001**, *17*, 5721.
(15) Hanley, L.; Choi, Y.; Fuoco, E. R.; Akin, F. A.; Wijesundara, M. B. J.; Li, M.; Tikhonov, A.; Schlossman, M. *Nucl. Instrum. Methods Phys. Res., Sect. B* **2003**, *203C*, 116.
(16) Kiely, J. D.; Bonnell, D. A. *J. Vac. Sci. Technol., B* **1997**, *15*, 1483.
(17) Parratt, L. G. *Phys. Rev.* **1954**, *95*, 359.
(18) Allen, M. P.; Tildesley, D. J. *Computer Simulation of Liquids*; Oxford University Press: New York, 1987.
(19) Brenner, D. W.; Shenderova, O. A.; Harrison, J. A.; Stuart, S. J.; Ni, B.; Sinnott, S. B. *J. Phys.: Condens. Matter* **2002**, *14*, 783.
(20) Jang, I.; Sinnott, S. B. *J. Phys. Chem. B*, submitted for publication, 2004.
(21) Schwickert, H.; Strobl, G.; Kimmig, M. *J. Chem. Phys.* **1991**, *95*, 2800.
(22) Fuoco, E. R.; Hanley, L. *J. Appl. Phys.* **2002**, *92*, 37.
(23) Burroughs, J. A.; Hanley, L. *Anal. Chem.* **1994**, *66*, 3644.
(24) Ni, B.; Andrews, R.; Jacques, D.; Qian, D.; Wijesundara, M.; Choi, Y.; Hanley, L.; Sinnott, S. B. *J. Phys. Chem. B* **2001**, *105*, 12719.
(25) Jang, I.; Ni, B.; Sinnott, S. B. *J. Vac. Sci. Technol., A* **2002**, *20*, 564.
(26) Tepavcevic, S.; Choi, Y.; Hanley, L. *J. Am. Chem. Soc.* **2003**, *125*, 2396.